RSC Advances

Operating temperature dependent ethanol and formaldehyde detection of spray deposited mixed CdO and MnO2 thin films

Journal:	*RSC Advances*
Manuscript ID:	RA-ART-01-2015-000734.R3
Article Type:	Paper
Date Submitted by the Author:	17-Apr-2015
Complete List of Authors:	Chandiramouli, R.; SASTRA University, SEEE Jeyaprakash, B.G.; SASTRA University, CeNTAB

Operating temperature dependent ethanol and formaldehyde detection of spray deposited mixed CdO and MnO_2 thin films

R. Chandiramouli[1] and B. G. Jeyaprakash[1, 2*]

[1]School of Electrical & Electronics Engineering

[2]Centre for Nanotechnology & Advanced Biomaterials

SASTRA University, Thanjavur -613 401, India

***Corresponding Author:**

Dr. B.G. Jeyaprakash

School of Electrical & Electronics Engineering and

Centre for Nanotechnology & Advanced Biomaterials

SASTRA University, Thanjavur -613 401, India

Tel.:+91-98654-21411

E-mail: **jp@ece.sastra.edu**

Abstract

The CdO-MnO_2 mixed oxide films are synthesized using spray pyrolysis method. The structural study confirms polycrystalline nature of the film and also confirms that the films are in mixed oxide state. The morphological study reveals that the crystallite sizes are around 30 nm to 40 nm with spherical morphology. Energy dispersive spectroscopy confirms the presence of cadmium, manganese and oxygen in mixed oxide state. The prepared CdO-MnO_2film is highly sensitive to ethanol vapours at ambient temperature. The resistance of the film decreases drastically when exposed to ethanol and formaldehyde vapours. The prepared CdO-MnO_2 is highly sensitive to ethanol at ambient temperature and for formaldehyde vapour at 393 K. The sensitivity, selectivity, response time, recovery time and stability of CdO-MnO_2 film towards ethanol and formaldehyde sensing are reported in the present work.

Keywords: Mixed oxide, Nanostructure, Sensitivity, Selectivity, Response time, Recovery time

1. Introduction

Metal oxide semiconductors such as SnO_2, ZnO, Bi_2O_3, TiO_2, Ga_2O_3, Fe_2O_3 are widely used for the detection of toxic gases such as CO, H_2S, NO_2 and volatile organic compounds (VOCs) such as CH_4, C_2H_5OH, C_3H_8, benzene, acetone etc.[1-8] Conductometric sensors based on metal oxides are commonly used as gas sensors to monitor toxic vapours in the environment. When the threshold limit of these toxic gases or vapours exceeds it will have harmful effects on humans and also to the ecosystem. The gas sensing mechanism of metal oxide type gas sensors involves the chemisorption of oxygen from air atmosphere on to the base material creating the space charge layer around the nanostructure in the base material, when the target gas molecules interacts with chemisorbed oxygen on metal oxide results in charge transfer to takes place between the base material and oxygen resulting in change in the surface resistance of sensing element.[9] However, the gas sensing properties of metal oxide varies due to various factors such as morphology, nano-dimension, porosity, catalytic activity, surface chemical properties and activation energy.[10-16] The sensitivity and selectivity of target gas to a particular material is a challenging task in gas sensing. Nevertheless, most of the mechanism involves between the adsorbed oxygen and target gas, the working temperature is usually high to activate the sensing process. To overcome all these difficulties and to enhance the sensing properties towards the gas or vapour there is need for smart gas sensor which can be operated at ambient temperature with enhanced sensing response. Based on these aspects, literature survey was conducted and it is inferred that most of the reported works are in gas sensing studies on metal oxide thin films or nanoparticles towards target gas.[17-20] We have reported the ethanol sensing properties of cadmium oxide.[21] To date, not much work has been reported based on cadmium oxide (CdO) and manganese oxide (MnO_2) on ethanol and formaldehyde vapour sensing. The novel aspect of the

present work is to enhance the sensing properties towards ethanol and formaldehyde with nanostructured mixed oxide (CdO-MnO_2) thin film. The CdO-MnO_2 mixed oxide is highly sensitive towards ethanol and formaldehyde at different operating temperatures. The sensing properties are fine-tuned by synthesizing the mixed oxide CdO-MnO_2 in nanostructured form. In the present work, CdO and MnO_2 thin films are synthesized and the vapour sensing characteristics are studied and reported.

2. Materials and methods

2.1 Thin film preparation

Mixed oxides of cadmium oxides and manganese oxides are deposited onto the glass substrate by home-built spray pyrolysis unit.[22] Cadmium acetate dihydrate [$(CH_3COO)_2Cd.2H_2O$, 99.9% purity, Nice] is used as precursor salt of 0.05M is dissolved in 25 mL deionized water. Manganese acetate tetrahydrate [$(CH_3COO)_2Mn.4H_2O$, 99.9% purity, Qualigens] is used as precursor salt of 0.05 M is dissolved in 25 mL deionized water. Then both solutions are mixed together to make up a solution of 50mL and stirred in the magnetic stirrer for half an hour for the preparation of precursor solution. The precursor solution is then atomized as a fine mist by air compressor through a glass nozzle and sprayed on to the pre-heated glass substrate at an angle of 45^o. The temperature of the glass substrate is maintained at a temperature of 230 ± 1^oC with a thermostat fitted with K-type thermocouple. Many samples are deposited by varying the substrate temperature and for different thickness to find the optimized condition for uniform distribution of nanocrystallites over the glass substrate. Finally, it was observed that for the deposition temperature of around 230^oC, the precursor solution vaporizes and uniform thin film is deposited on the glass substrate. For low substrate temperature the deposition results in incomplete pyrolytic reaction with partial decomposition of precursor salt. Hence, for uniform

coating of mixed oxides the substrate temperature is maintained at 230^{o}C. The compressed dry air with a pressure of 2kg/cm^{2} is used as carrier gas and the distance between the glass substrate and atomizer is maintained at a distance of 30 cm. In order to obtain a uniform coating the precursor solution is sprayed onto the glass substrate with the time duration of 5 s at an interval of 60 s.

2.2 Characterization

Structural studies for the mixed oxide (CdO-MnO_2) film is carried out using Bruker – D8 Focus X-Ray Diffraction (XRD) Unit with Cu Kα_1 radiation with the generator setting of 30 mA and 40 kV. The surface morphology and elemental identification of the film are obtained from JEOL-6701 Field-Emission Scanning Electron Microscopy (FE-SEM) with Energy dispersive X-ray analysis (EDAX) detector. The optical studies of mixed oxide CdO-MnO_2thin films were carried out using UV-Visible spectrophotometer (Perkin Elmer Lamda 25). The film thickness is measured by stylus profilometer (Mitutoyo SJ 301) and the thickness of the mixed oxide CdO-MnO_2 films is found to be around 500 nm.

2.3 Vapour sensing setup

For vapour sensing studies, home-built vapour sensing unit is used with thermostat. The capacity of the test chamber is 1.5 L. Initially, the thin film is conditioned at 300^{o}C for 24 hours to remove the water molecules and unwanted organic materials. The ohmic contacts are made on to the thin film (12mm x 10 mm) with thin copper wire and silver epoxy. The change in the electrical resistance of the film is recorded using National Instruments Data Acquisition board (NI DAQ 6212) during the process of injecting and evacuating ethanol and formaldehyde vapours. The dry ethanol is procured from Sigma-Aldrich [Pure, anhydrous, ≥99.5%, 459836] and used as such without further purification. The electrical resistance of thin film in dry air is in

the order of GΩ and this resistance is taken as the baseline resistance (R_o) in the present study. For sensing studies, calibrated volume of ethanol and formaldehyde is introduced into the test chamber and the response of the film towards the vapours is studied.

2.4 Computational details

In the proposed model, mixed oxide CdO-MnO_2 is taken as scattering region between two gold electrodes. The left electrode is kept at two volts and the right electrode is kept at constant ground potential. The proposed model is constructed and optimized using TranSIESTA module in SIESTA package. In SIESTA code, the core electrons are replaced by pseudopotentials. The generalized gradient approximation (GGA) with Perdew-Burke-Ernzerhof (PBE) exchange correlation functional is used during calculation. The Brillouin zones are sampled with 1 x 1 x 100 k points in the present model. The optimization of molecular device is carried out with single zeta polarization for gold atoms and double zeta polarization for cadmium, manganese and oxygen atoms in the present model.

3. Results and discussion

3.1 Structural studies

The X-ray diffraction (XRD) pattern of mixed oxide CdO-MnO_2 is shown in Fig. 1. The orientation of planes for both CdO and MnO_2 confirms the polycrystalline nature. The peaks at different 2θ values exactly matches with JCPDS card number 05-0640 for CdO and JCPDS card number 42-1169 for MnO_2. This also confirms that the prepared films are not ternary compound but in mixed oxide state. The crystallite size was estimated using known Scherrer formula,

$$D = \frac{S \times \lambda}{\beta \times \cos\theta} \text{----------(1)}$$

where *D* represents the crystallite size (nm), *S* denotes the shape factor which is equal to 0.9, λ is X-ray wavelength (1.5406 Å), θ is the diffraction angle (radians) and β is full width at half maximum (FWHM in radians). The X-ray line broadening clearly infers that the crystallite of CdO-MnO_2 is in nanometric regime. The calculated crystallite size of CdO-MnO_2 mixed oxide is found to be around 30 nm to 40 nm from the Scherrer formula.

3.2 Morphological studies and elemental analysis

Fig. 2 represents the field-emission scanning electron micrograph (FE-SEM) of mixed oxide CdO-MnO_2 thin film. The synthesized film exhibits the spherical morphology with porosity. For the optimized preparatory condition with respect to concentration of precursor solution and substrate temperature, the prepared CdO-MnO_2 film shows spherical like morphology. The formation of worm-like structure is due to the influence of electrostatic mechanism, which arises due to the possibility of exchange of free electrons between nanocrystallites among small intercrystallite distances.[23] The crystallite size of prepared films is observed to be around 30nm to 40nm which is also in good agreement with the calculated value of crystallite size using Scherrer formula in XRD. Fig. 3 illustrates the energy dispersive X-ray analysis (EDAX) spectrum. It is clearly inferred that the synthesized mixed oxide film shows the presence of elements cadmium, manganese, oxygen and silicon. The presence of element silicon in the spectrum is due to glass substrate. Since the atomic number of cadmium is forty eight, Lα line in EDAX spectrum is observed near 3.2 eV. Moreover, for manganese and oxygen Kα lines are observed in lower energies. Fig. 4 depicts the mapping of elements for the prepared film. It is clearly observed that in the mixed configuration, the elements oxygen, silicon, manganese and cadmium are noticed (color gradient shows the presence of elements). The positions of individual elements in thin films are mapped separately. From the map, it is clearly inferred that

the formed thin film is in mixed oxide state with CdO and MnO_2 and not as a ternary compound. The map of elements in EDAX spectrum is in good agreement with XRD which also confirms the mixed oxide state of the film.

3.3. Optical studies

The optical properties for the mixed oxide CdO-MnO_2 are studied within the wavelength range of 300 nm to 1100 nm. The visual appearance of the prepared film is glassy black in color. The transmittance of mixed oxide CdO-MnO_2 is shown in Fig. 5. The transmittance of the film is in the order of 20% to 50% in the visible region. The drastic variation in transmittance is observed for CdO-MnO_2 mixed oxide film in visible region. Moreover, the transmittance increases to nearly 70% in the infra-red region. The low magnitude of transmission in the visible region supports the polycrystalline nature of the film with high surface roughness, which is a favorable condition for chemical sensors.[24] The optical band gap of the CdO-MnO_2 mixed oxide film is obtained from Tauc's plot and is depicted in Fig. 6. The optical band gap of MnO_2 are reported as 2.5 eV and for CdO[25], the reported optical band gap is around 2.3 eV.[21] However, in the mixed oxide state of CdO-MnO_2, the optical band gap increases to 2.7 eV.

3.4 Ethanol vapour sensing mechanism

Ethanol is a colorless, inflammable volatile organic compound found in alcoholic beverages.[26, 27] The use of ethanol also wide spread in medicine, chemical industry and in food industry.[28, 29] Ethanol causes the harmful effects in human which depends on the concentration. The higher dose of ethanol vapours results in mild euphoria to severe depression in central nervous system.[30] This necessitated the detection level of ethanol in the order of parts per million (ppm) level. At first, the mixed oxide CdO-MnO_2 film is exposed to air atmosphere, the oxygen molecules are adsorbed as molecular oxygen ions O_2^- at low temperatures as given in Eq. (2),

$$O_2 + e^- \xrightarrow[CdO-MnO_2\ surface]{} O^-_{2\,(ads)} \quad \text{----------} \quad (2)$$

When the mixed oxide CdO-MnO_2 films is exposed to ethanol vapours, nanocrystallites of CdO-MnO_2 present on the surface shows a catalytic activity[31] with the exothermic reaction between the adsorbed oxygen ions and ethanol and can be represented as Eq. 2. We have reported the ethanol sensing characteristics of CdO thin film.[21] However, the ethanol sensing is feasible only at the temperature of 523 K. The ethanol sensing response for pure CdO and pure MnO_2 thin films is found to be around 0% at ambient temperature. In contrast, the response is optimum in the mixed oxide state for ethanol sensing. The adsorbed oxygen ions in the mixed oxide film are desorbed by oxidation of ethanol vapours. The consumed electrons by the oxygen ion from the conduction of the mixed oxide films are released back to the mixed oxide film which decreases the resistance of the film. This process reduces the electrical resistance of the mixed oxide CdO-MnO_2 film. This change in the resistance of the mixed oxide film is utilized in detecting the ethanol vapours. The oxidation of ethanol vapours takes place in the ambient air.[32,33] For the catalytic activity to take place, usually activation energy is required in the form of thermal energy or optical energy. Interestingly, in the case of mixed oxide CdO-MnO_2 thin film, it shows the response at ambient temperature for ethanol vapours.

$$C_2H_5OH + 3O^-_{2\,(ads)} \xrightarrow[CdO-MnO_2\ surface]{} 2CO_2 \uparrow + 3H_2O \uparrow + 3e^- \quad \text{----------} \quad (3)$$

The sensing response of mixed oxide CdO-MnO_2 can be estimated using the following expression as

$$\%\ S = \frac{\left(R_o - R_g\right)}{R_g} \times 100 \quad \text{----------} \quad (4)$$

where R_o and R_g are the electrical resistance of the film in the presence of air and in presence of ethanol vapour under dry-air atmosphere respectively. The sensing response of mixed oxide CdO-MnO_2 increases enormously with increase in ethanol concentration as shown in Fig. 7. The electrical resistance of the mixed oxide film at ambient air is around 1GΩ. However, when CdO-MnO_2 film is exposed to ethanol vapours, the resistance of mixed oxide film drastically decreases to 0.625 GΩ for 15 ppm concentration. Besides, increase in the concentration of ethanol result in decrease of resistance to 0.55 GΩ.

Fig. 8a-b illustrates the proposed model of CdO-MnO_2 mixed oxide two probe molecular device. The adsorption characteristics of ethanol are carried out on different sites of CdO-MnO_2 scattering region. The current-voltage characteristics of the proposed model are studied in this state. Moreover, when ethanol gets adsorbed on cadmium site, there is no significant response. Interestingly, in the optimized condition, when hydroxyl group in the ethanol molecule gets adsorbed on to manganese atom of mixed CdO-MnO_2, the response increases. This clearly infers that when ethanol molecule gets adsorbed on to the mixed oxide, transfer of electrons takes place between the mixed oxide and ethanol which is confirmed with change in the current.[34,35] The theoretical model also supports that in the mixed oxide state the transfer of electrons increases which in turn is observed by the increase in the current. The proposed model is used to validate the experimental results of the present work. The response towards ethanol is not significant in pure CdO and pure MnO_2 at ambient temperature. Despite, in mixed oxide state, the response is more promising, which can be highlighted that only in mixed oxide state ethanol gets oxidized and dissociates in the base material. However, the present study is carried out for ethanol on CdO-MnO_2 scattering region only at ambient temperature. Due to constraints in software

package, the study is not carried out at elevated temperature. Moreover, in future the proposed model may be extended for elevated temperature.

3.5. Response and recovery studies of Ethanol

The transient resistance response of mixed oxide CdO-MnO_2 thin film is investigated with ethanol vapour concentration ranging from 15 ppm to 75 ppm at ambient temperature (300 K). Fig. 9 depicts the transient response of CdO-MnO_2 films towards various concentrations. However, on increasing the ethanol concentration the resistance drops further to the low value. Moreover, beyond the concentration of 75 ppm there is not much variation in the resistance. This shows that for higher concentration ethanol vapours completely depletes the grains in the mixed oxide film and there is no further decrease in the resistance. This infers that the prepared mixed oxide CdO-MnO_2 film can be used to detect ethanol vapour in the order of 15 ppm to 75 ppm. Fig. 10 represents the repeatability curve of ethanol for 30 ppm; it clearly signifies that for different cycles of operation the trend in the variation of resistance is almost same. Fig. 11 shows the response time and recovery time versus concentration of ethanol vapours. It indicates the fast response time and a slow recovery time when the concentration of ethanol increases. For small crystallite size of 30 nm to 40 nm, it leads to rapid response-recovery behavior in the order of seconds. For lower concentrations, desorption of oxygen ions requires more time so the response time is more. In contrast, for higher concentrations, the vapour rapidly desorbs oxygen ions and the response time is rapid.[36] However, for recovery time it takes more time since the ethanol are completely depleted over the crystallites in the mixed oxide film. Fig. 12 represents the sensing response and selectivity of CdO-MnO_2 mixed oxide for ethanol and various other volatile organic compounds (VOCs) at ambient temperature of 300 K. The sensor response for 15 ppm ethanol is around 61 % compared with other VOCs such as formaldehyde, acetone, CCl_4 and

1,2dichloroethylene. When the concentration of ethanol and other VOCs increases the response also increases. However, CdO-MnO_2 mixed oxide film is highly sensitive and selective towards ethanol vapours than other VOCs at ambient temperature. Moreover, for higher concentration of ethanol, the mixed CdO-MnO_2film shows better response. From the response to other VOCs plot, it can be concluded that the prepared mixed oxide CdO-MnO_2 is highly sensitive towards ethanol vapour at ambient temperature. Table 1 represents the ethanol sensing studies of different chemiresistive sensors.[37-43] In previously reported work the response and recovery time is more or the sensor is operated at high temperature for sensing ethanol vapours. However, in the present work mixed oxide CdO-MnO_2 thin film is employed for ethanol sensing with short response and recovery time. Moreover, CdO-MnO_2 can detect ethanol vapours at ambient temperature. The other point to be highlighted is at ambient temperature the sensor response increases to 80% for ethanol which can be concluded that CdO-MnO_2 mixed oxide can be used as a reliable sensor to detect ethanol vapour in the mixed gas environment.

3.6 Formaldehyde vapour sensing mechanism

Formaldehyde is one of the carcinogens which are found in formalin solutions, condensation of polymerization used in paints and building materials and in industrial chemical process.[44-46] Occupational Safety and Health Administration (OSHA) has set the threshold level of 20 ppm. Thus monitoring the formaldehyde level in air atmosphere is important for human health. Initially the mixed oxide film of CdO-MnO_2 is exposed to air, for oxygen to get adsorbed on to the film surface as represented in Eq. (1). As such, when the mixed oxide film is exposed to formaldehyde, the decrease in the width of the depletion region occurs across the crystallite resulting in the decrease in film resistance. The catalytic activity will increase the number of oxygen adsorption over the mixed oxide film surface which enhances the formaldehyde sensing

characteristics. However, the formaldehyde sensing is enhanced only when the activation energy is given in the form of thermal energy. Moreover the sensing mechanism of formaldehyde is more favorable only at a temperature of 393 K. At ambient temperature, the catalytic activity is not favorable for formaldehyde sensing however good for ethanol. The response towards formaldehyde sensing is nearly 0% for pure CdO and pure MnO_2 thin films. Fig. 13 represents resistance and response versus concentration plot. It is clearly observed under ambient air atmosphere, the film resistance is around 6 GΩ, upon exposure to formaldehyde vapours and it decreases the resistance to 4.29 GΩ for 30 ppm concentration. Further increase in the concentration to 90 ppm makes the resistance of the film to drop drastically to 1 GΩ. The response of the mixed oxide film increases from 37 % for 30 ppm to 600 % for 90 ppm concentration. From the observation it is clearly inferred that CdO-MnO_2 mixed oxide film can be used as a chemiresistor for efficient formaldehyde detection.

3.7 Response and recovery studies of Formaldehyde

Fig. 14 illustrates the transient response of CdO-MnO_2 film for different concentration. Usually the metal oxide semiconductor based vapour detection is not linear for the wide range of vapour concentration. This is because of measurement method, carrier injection due to reducing process and operating temperature. In the present studies, we observed that above 30 ppm, a significant change in electrical resistance and may be due the injected number of carrier concentration which is high. To measure this electrical resistance, the film has to be biased with constant current / voltage. In the present studies the measurement were made by fixing the voltage of 20Vdc. Hence, below this concentration much variation may not be observed and called as the dead band. However, increase in operating temperature for detection of formaldehyde is necessary to activate the process; the optimum temperature for formaldehyde

sensing is around 393 K. The fine crystallites of CdO-MnO_2 increase the sensitivity for higher concentrations of formaldehyde. As soon as the formaldehyde vapours are evacuated, the film reaches its baseline resistance. Fig. 15shows the repeatability curve of formaldehyde vapour sensing at a concentration of 30 ppm at 393 K. The change in resistance is clearly observed upon exposure of formaldehyde vapour on CdO-MnO_2 film. Moreover, the paths traced during the cycles of operations are similar. Fig. 16 illustrates the response time, recovery time versus concentration of formaldehyde vapours. For lower concentration of 30 ppm, the response time is around 30 seconds, on increasing formaldehyde concentration to 90 ppm, the response time significantly decreases to 9 seconds at the temperature of393 K. This clearly indicates that at higher concentration, desorption of oxygen ions are more favorable. In contrast, the recovery time increases due to the complete depletion of grains with formaldehyde vapours. The response time and recovery time is in the order of seconds which infers that the prepared mixed oxides of CdO-MnO_2 are highly sensitive towards formaldehyde vapours. Fig. 17 refers the sensing response and selectivity of formaldehyde towards other interfering vapours. The response is around 600% for 90 ppm of formaldehyde vapours. Besides, the response of other reducing vapours is less than 100 % for 90 ppm this clearly indicates that CdO-MnO_2 film is highly selective towards formaldehyde vapours. From the selectivity plot it is inferred that even in mixed vapour environment the mixed oxide film is sensitive to formaldehyde vapours. Table 2 compares the formaldehyde sensing parameters with different types of nanostructured HCHO sensors.[47-51] From the previous reports it is inferred for formaldehyde sensing; the response-recovery time is long. However, selectivity towards formaldehyde than other vapours is also a challenging task. Moreover, in the present work mixed CdO-MnO_2 thin film is used to detect formaldehyde vapour at 393 K with enhanced selectivity. Analyzing all these factors it can be

concluded that CdO-MnO_2 mixed oxide film is a promising material to detect formaldehyde vapours. Fig. 18 represents the response of ethanol and formaldehyde vapour for different temperature. It is clearly evident from the plot that response is appreciable for ethanol for ambient temperature. For higher temperature, the response is observed to be high for formaldehyde vapours. Fig 19 shows the response of pure CdO and pure MnO_2 films towards ethanol and formaldehyde at 300 K and 393 K. For pure CdO and pure MnO_2 film the response is around 0 % at 300 K. However, for pure CdO at 393 K the response to ethanol is 3 % and response to formaldehyde is 1 % and for pure MnO_2 film it is around 0 % for both ethanol and formaldehyde vapours. At high temperature, the ethanol may partially get dissociated before oxidation. Hence the response at elevated temperature decreases for mixed oxide film.

3.8 Stability and reproducibility of mixed oxide CdO-MnO_2 film

The sensing stability and reproducibility of mixed oxide CdO-MnO_2 are studied for 45 ppm concentration of ethanol and formaldehyde vapours at 300 K and 393 K respectively. Fig. 20 represents the stability of CdO-MnO_2 thin film as a function of time for 45 ppm ethanol and formaldehyde vapour. The measurement is carried out for a period of 180 days in intervals of 30 days. The response of mixed oxide CdO-MnO_2 film remains steady for ethanol and formaldehyde vapours. The response for ethanol is in the order of 75 % at ambient temperature, whereas for formaldehyde the response is in the order of 60 % at the temperature of 393 K. This confirms that the prepared film is stable and reproducibility can be attained over the period of time.

3.9 Humidity effect on sensing properties of mixed CdO-MnO_2 film

Relative Humidity (RH) plays an important role in the sensing characteristics of mixed CdO-MnO_2 film at ambient temperature. The influence of humidity on the sensing properties of ethanol and formaldehyde on mixed CdO-MnO_2 film is studied by creating humid environment

using saturated salt solutions namely KCl, NaCl and $MgCl_2$ solutions (RH = 84%, 75% and 33% respectively) in the vapour sensing chamber and RH is measured with hygrometer (RH of $\pm$ 1% is maintained). Upon exposing the film towards humid air, two mechanisms may take place; the water molecule gets adsorbed over the surface of film in molecular or hydroxyl form, which further donates the electrons to nanocrystallites. In other way, water molecule replaces the adsorbed oxygen ions and releases the electrons from the ionized oxygen atoms. In the above two mechanisms, the donor effect results to increase in the electron concentration in the conduction band of and decreases the electrical resistance of the film. The sensing response of the film for different humidity levels is calculated using Eq. (5) as,

$$\% S_{RH} = \frac{\left(R_{RH} - R_{RH+vapour}\right)}{R_{RH+vapour}} \times 100 \quad \text{----------(5)}$$

Where R_{RH} and $R_{RH+vapour}$ represents the resistance of the mixed oxide film in humid air and humid + vapour (ethanol or formaldehyde) environment respectively. Fig. 21 represents the ethanol and formaldehyde sensing response at different relative humid environment. The vapour sensing response of mixed CdO-MnO_2 decreases upon increase in RH. For low RH, water molecules chemisorb on oxygen vacant sites, which in turn decrease the response. Moreover, for high RH, the water molecules may be physisorbed due to capillary condensation. This significantly decreases the interaction of ethanol and formaldehyde in the film surface, further decreases the response.

4. Conclusion

The mixed oxide CdO-MnO_2 thin films are synthesized using home-built spray pyrolysis unit. The crystallinity and mixed oxides states of thin films are confirmed with XRD and EDAX results. When CdO-MnO_2 film is exposed to ethanol vapours, the film resistance decreases

drastically. The optimum concentration of ethanol vapours ranges from 15 ppm to 75 ppm at ambient temperature. The prepared CdO-MnO_2 is highly selective towards ethanol at ambient temperature than other vapours. The prepared CdO-MnO_2 is highly sensitive to ethanol vapours at the operating temperature of 300 K. At 393 K, CdO-MnO_2 film is highly selective towards formaldehyde than other interfering vapours. The response of CdO-MnO_2 is optimum for the concentration of 30 ppm to 90 ppm for formaldehyde. From the results it is concluded that the mixed oxide CdO-MnO_2 film can be used for ethanol and formaldehyde sensing.

Acknowledgements

The authors would like to acknowledge SASTRA University for facilitating the research work. The authors are thankful to Computational Nanoscience and Technology Lab. (CNTL), ABV-Indian Institute of Information Technology and Management, Gwalior for providing computational facilities.

Figure captions

Fig. 1. X-ray diffraction pattern of CdO-MnO_2 mixed oxide film.

Fig. 2. Field-emission scanning electron micrograph of CdO-MnO_2 mixed thin film.

Fig. 3. Energy dispersive X-ray spectrum of CdO-MnO_2 mixed oxide thin film.

Fig. 4. Elemental mapping of CdO-MnO_2 mixed oxide film.

Fig. 5. Optical transmittance spectrum of CdO-MnO_2 mixed oxide thin film.

Fig. 6. Tauc's plot of CdO-MnO_2 mixed oxide thin film.

Fig. 7. Variation in electrical resistance and sensing response of CdO-MnO_2 thin film for various ethanol concentrations at 300 K.

Fig. 8 (a) CdO-MnO_2 molecular device model with gold electrodes (b) Adsorption of ethanol molecule on manganese atom in CdO-MnO_2 molecular device.

Fig. 9. Transient response of CdO-MnO_2 films towards various concentrations of ethanol.

Fig. 10. Resistance repeatability plot of CdO-MnO_2 film for 30 ppm of ethanol.

Fig. 11. Response time and recovery time of the film versus concentration of ethanol.

Fig.12. Sensing response and selectivity of CdO-MnO_2 mixed oxide thin film towards various concentrations of ethanol and other volatile organic compounds at 300K.

Fig. 13. Variation in electrical resistance and sensing response of CdO-MnO_2 thin film for various formaldehyde concentrations at 393 K.

Fig. 14. Transient response of CdO-MnO_2 films towards various concentrations of formaldehyde.

Fig. 15. Resistance repeatability plot of CdO-MnO_2 film for 30 ppm formaldehyde.

Fig. 16. Response time and recovery time versus concentration of formaldehyde.

Fig. 17. Sensing response and selectivity of CdO-MnO_2 mixed oxide thin film towards various concentrations of formaldehyde and other volatile organic compounds at 393 K.

Fig. 18. Response of ethanol and formaldehyde plot for different temperature.

Fig. 19. Response of pure CdO and pure MnO_2 films to ethanol and formaldehyde.

Fig. 20. Stability of CdO-MnO_2 thin film as a function of time for 45 ppm ethanol and formaldehyde vapour.

Fig. 21. Ethanol and formaldehyde vapour response in different relative humid environment at 300 K

Table captions

Table.1 Comparison of ethanol sensing characteristics of chemiresistive sensors with the present work.

Table.2 Comparison of formaldehyde sensing characteristics of chemiresistive sensors with the present work.

References

1. M. Bagheria, A.A. Khodadadi, A.R. Mahjouba, Y. Mortazavi, *Sensors Actuators B Chem.,* 2013, **188,** 45– 52.
2. M.K. Verma, V. Gupta, *Sensors Actuators B Chem.*, 2012, **166-167**, 378-385.
3. A. Mortezaali, R. Moradi, *Sensor Actuators A,*2014, **206**, 30-34.
4. M. Hjiri, R. Dhahri, K. Omri, L. Elmir, S.G. Leonardi, N. Donato, G. Neri, *Mater. Sci. Semicond. Process.* 2014, **27**, 319-325.
5. A. Cabot, A. Marsal, J. Arbiol, J.R. Morante, *Sensors Actuators B Chem.*, 2004,**99,** 74-89.
6. Y. Gönüllü, G. César, M. Rodríguez, B. Saruhana, M. Ürgen, *Sensors Actuators B Chem.,*2012, **169,** 151-160.
7. M.R. Mohammadi, D.J. Fray, *Acta Mater.*2007, **55**, 4455-4466.
8. S.T. Navale, G.D. Khuspe, M.A. Chougule, V.B. Patil, *Ceram. Int.,*2014, **40**, 8013-8020.
9. M.N.Rumyantseva, E.A. Makeeva, A.M. Gas'kov, *Russ. J. Gen. Chem.* 2008, **78,** 2556-2565.
10. N.A. Beckers, M.T. Taschuk, M.J. Brett, *Sensors Actuators B Chem.*,2013, **176,**1096-1102.
11. I.C. Hurtado, G.G. Mandayo, E. Castaño, *Thin Solid Films,*2013, **548,**665-676.
12. S. Das, V. Jayaraman, *Prog. Mater Sci.,*2014, **66**, 112-255.
13. G. Korotcenkov, B.K. Cho, *Sensors Actuator B Chem.,* 2009, **142**, 321-330.
14. A. Cabot, A. Vila , J.R. Morante, *Sensors Actuators B Chem.*2002, **84,** 12-20.
15. R.G. Pavelko, A.A. Vasiliev, E. Llobet, X. Vilanova, N. Barrabés, F. Medina, V.G. Sevastyanov, *Sensors Actuators B Chem.,*2009, **137**, 637-643.

16. M. Yao, F. Ding, Y. Cao, P. Hu, J. Fan, C. Lu, F. Yuan, C. Shi, Y. Chen, *Sensors Actuators B Chem.,* 2014,**201,** 255-265.

17. G. Korotcenkov, B.K. Cho, *Sensors Actuators B Chem.*, 2014, **196,** 80-98.

18. G. Korotcenkov, I. Boris, V. Brinzari, S.H. Han, B.K. Cho, *Sensors Actuators B Chem.*, 2013, **182**, 112-124.

19. K. Großmann, K.E. Kovács, D.K. Pham, L. Mädler, N. Barsan, U. Weimar, *Sensors Actuators B Chem.*, 2011, **158**, 388-392.

20. H.G. Moon, H.W. Jang, J.S. Kim, H.H. Park, S.J. Yoon, *Sensors Actuators B Chem.*,2011, **153**, 37-43.

21. R. Chandiramouli, B.G. Jeyaprakash, *Solid State Sci.,*2013, **16**, 102-110.

22. B.G. Jeyaprakash, K. Kesavan, R.A. Kumar, S. Mohan, A. Amalarani, *Bull. Mater.Sci.*, 2011, **34**, 601-605.

23. Norris, Charles P, Trends in Surface Science Research, Nova science publishers, Pub. Date: 2005, ISBN: 1-59454-178-7, page 88.

24. B. Kannan, R. Pandeeswari, B.G. Jeyaprakash, *Ceram. Int.,*2014, **40**, 5817-5823.

25. A.M. Toufiq, F. Wang, Q. Javed, Q. Li, Y. Li, *Appl. Phys. A.,* 2013, **116**, 1127-1132.

26. E. Karahanian, M.E. Quintanilla, L. Tampier, M.R. Meza, D. Bustamante, V. Gonzalez-Lira, et al., *Alcohol. Clin.Exp.Res.,*2011, **35,** 606–612.

27. D. Li, H. Zhen, L. Xingcai, Z.W. Gao, Y.J. Guang, *Renew. Energy*, 2005, **30**, 967-976.

28. S. Develi, B. Evran, E.B. Kalaz, N.K. Toker, G.Ö. Erata, *Chin. J. Nat. Med.,* 2014, **12,** 495–499.

29. J.L. Silveira, V.J. Martinelli, L.F. Vane, J.C.F. Junior, R.A.Z. Vigouroux, C.E. Tuna, et al., *Appl. Therm. Eng.,* 2014, **71**, 94-103.

30. Y.P. Lee, J.T. Liao, Y.W. Cheng, T.L. Wu, S.L. Lee, J.K. Liu, et al., *Alcohol.* 2013, **47**, 559-565.

31. G. Singh, I.P.S. Kapoor, R. Dubey, P. Srivastava, *Mater. Sci. Eng. B.,* 2011, **176,** 121-126.

32. K. Vijayalakshmi, S. David Jereil, *Ceramics International*., 2015, **41**, 3220–3226.

33. Shah Abdul Hakim, Yueli Liu, Yu Lu, Wen Chen, *Mat. Sci. Semicond. Proc.* 2015, **31**, 630–638.

34. Xing Liu, Bin Cheng, Jifan Hu, HongweiQin,*Com. Mater. Sci.,*2013,**68**, 90–94.

35. Pedro O. Bedolla,GregorFeldbauer,MichaelWolloch,ChristophGruber,Stefan J. Eder,NicoleDorr,PeterMohn,JosefRedinger, AndrasVernes, *J. Phys. Chem. C* 2014, **118**, 21428−21437.

36. G. Korotcenkov, *Mater. Sci. Eng. B.,* 2007, **139**, 1-23.

37. Y. Kwon, H. Kim, S. Lee, I.J. Chin, T.Y. Seong, W.I. Lee, et al., *Sensors Actuators B Chem.,* 2012, **173**, 441-446.

38. R. Pandeeswari, R.K. Karn, B.G. Jeyaprakash, *Sensors Actuators B Chem.,* 2014, **194,** 470-477.

39. P. Song, D. Han, H. Zhang, J. Li, Z. Yang, Q. Wang, *Sensors Actuators B Chem.*, 2014, **196,** 434–439.

40. S. Wei, S. Wang, Y. Zhang, M. Zhou, *Sensors Actuators B Chem.,* 2014, **192,** 480-487.

41. K.L.A. Kumar, S. Durgajanani, B.G. Jeyaprakash, J.B.B. Rayappan, *Sensors Actuators B Chem.*, 2013, **177**, 19-26.

42. S. Park, H. Ko, S. An, W.I. Lee, S. Lee, C. Lee, *Ceram. Int.,* 2013, **39**, 5255-5262.

43. D. Sivalingam, J.B. Gopalakrishnan, J.B.B. Rayappan, *Mater. Lett.,* 2012, **77**, 117-120.

44. R.C. Chautems, X. Delgadillo, J.P. Deleaval, B. Roche, et al., *Colorectal Disease,* 2003, xx, 24-28.

45. J. Lubczak, I.C. Cicirko, B. Mysliwiec, xxx, 2002, **53**,113-124.

46. H. Teng, S. Wang, *Carbon*, 2000, **38**, 817-824.

47. X. Chi, C. Liu, L. Liu, S. Li, H. Li, X. Zhang, et al., *Mater. Sci. Semicond. Process.,* 2014, **18,** 160-164.

48. W. Yang, P. Wan, X. Zhou, J. Hu, Y. Guan, L. Feng, *Sensors Actuators B Chem.,* 2014, **201,** 228-233.

49. K. Xu, D. Zeng, S. Tian, S. Zhang, C. Xie, *Sensors Actuators B Chem.,* 2014, **190**, 585-592.

50. Y. Zheng, J. Wang, P. Yao, *Sensors Actuators B Chem.,* 2011, **156,** 723-730.

51. L. Zhang, J. Zhao, J. Zheng, L. Li, Z. Zhu, *Appl. Surf. Sci.,* 2011, **258,** 711–718.

Fig. 1.

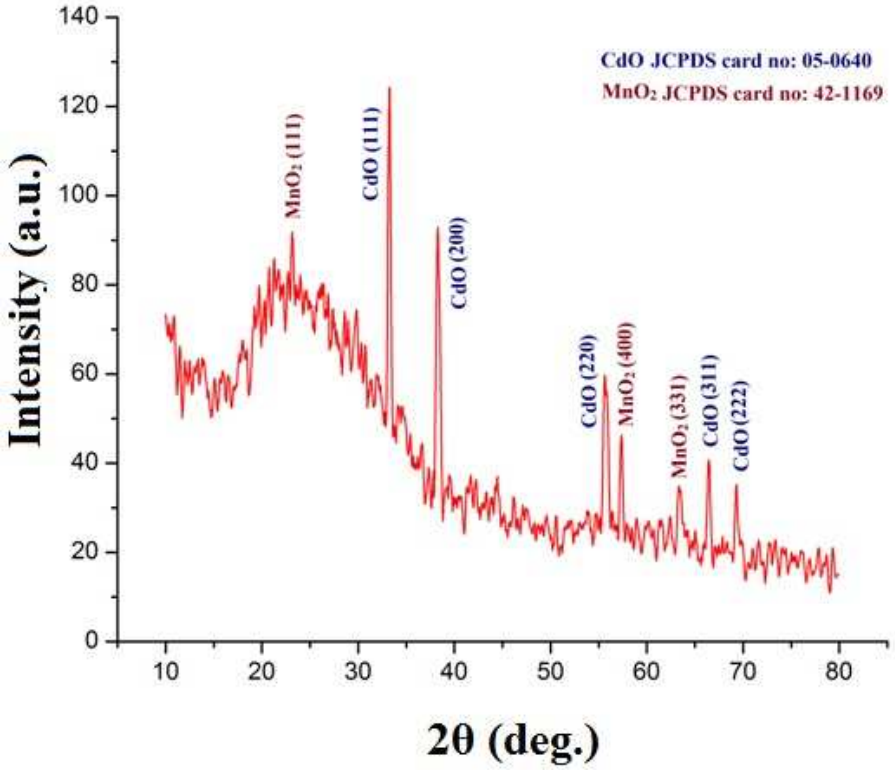
CdO JCPDS card no: 05-0640
MnO2 JCPDS card no: 42-1169
MnO2 (111)
CdO (111)
CdO (200)
CdO (220)
MnO2 (400)
MnO2 (331)
CdO (311)
CdO (222)
Intensity (a.u.)
2θ (deg.)
0
20
40
60
80
100
120
140
10
20
30
40
50
60
70
80

Fig. 2.

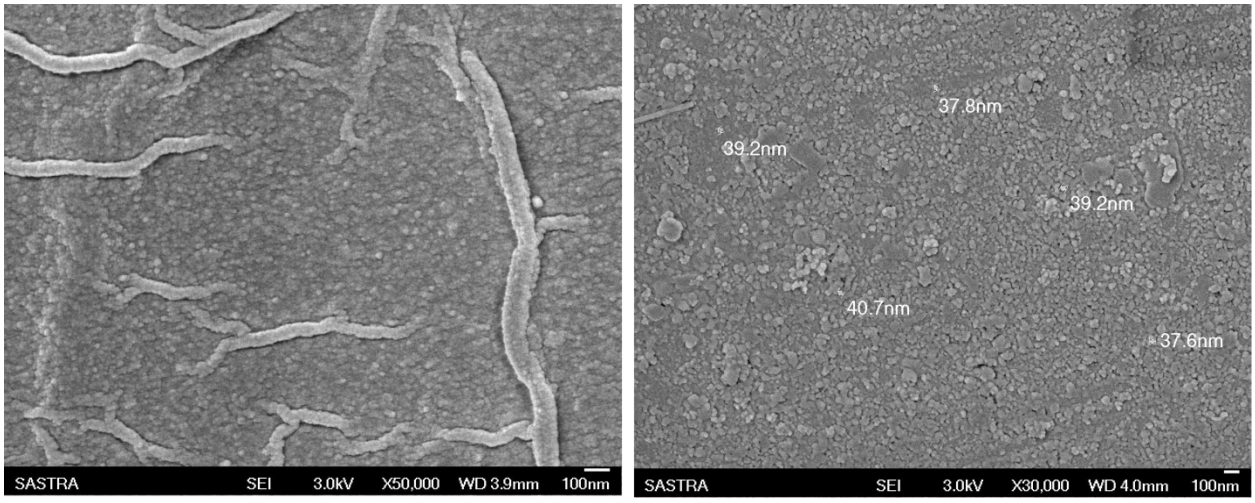
SASTRA SEI 3.0kV X50,000 WD 3.9mm 100nm
37.8nm
39.2nm
39.2nm
40.7nm
37.6nm
SASTRA SEI 3.0kV X30,000 WD 4.0mm 100nm

Fig. 3.

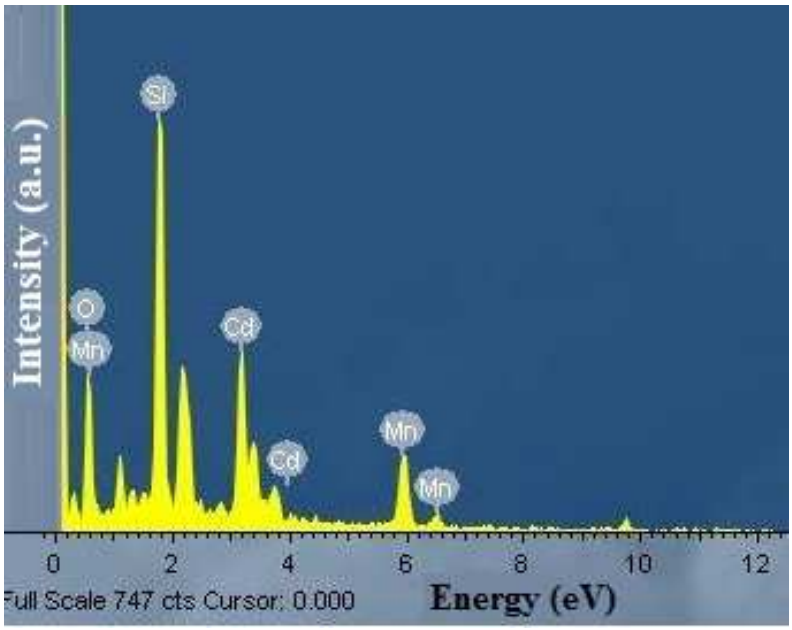
Intensity (a.u.)
Si
O
Mn
Cd
Cd
Mn
Mn
0
2
4
6
8
10
12
Full Scale 747 cts Cursor: 0.000
Energy (eV)

Fig. 4.

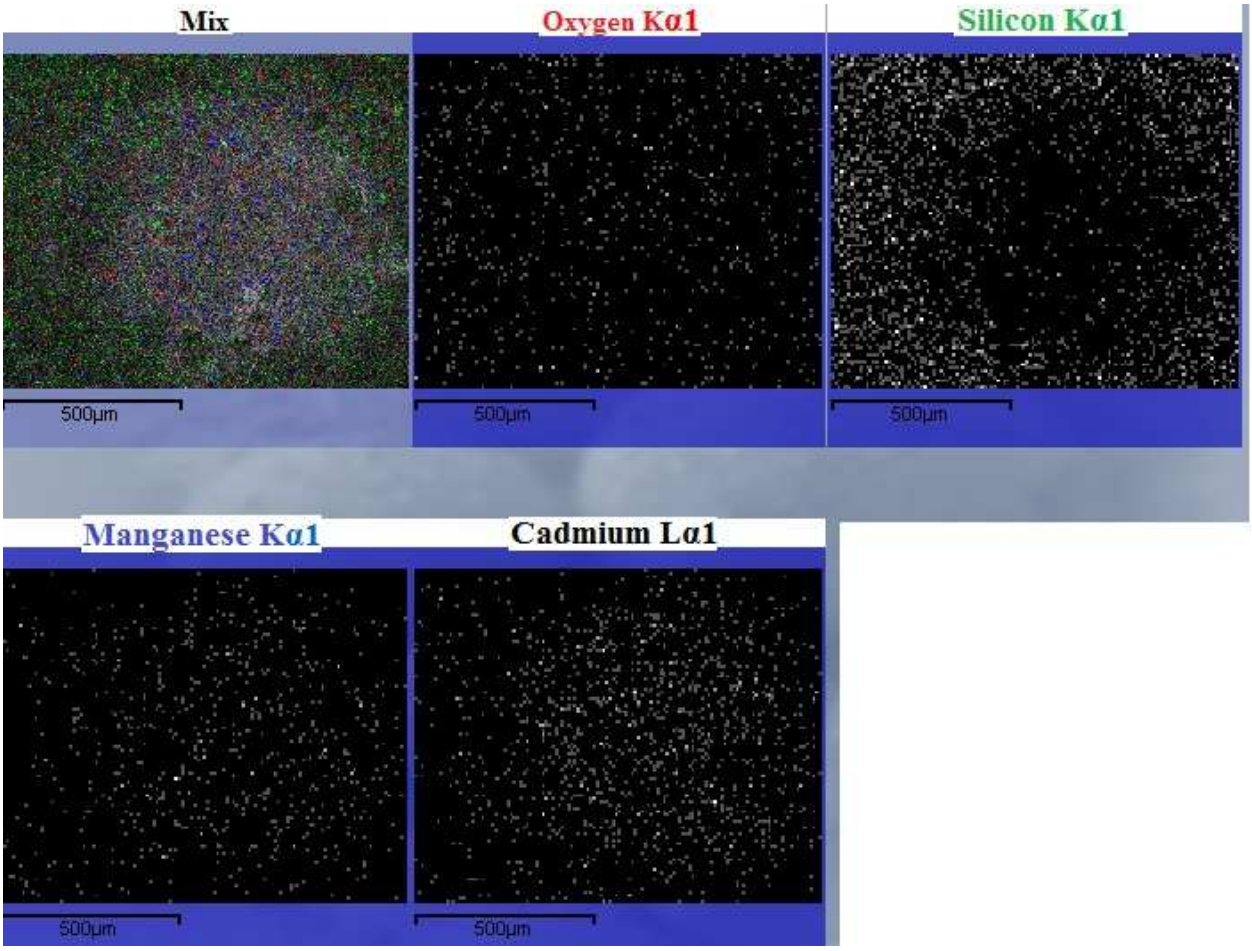
Mix
Oxygen Kα1
Silicon Kα1
500µm
500µm
500µm
Manganese Kα1
Cadmium Lα1
500µm
500µm

Fig. 5

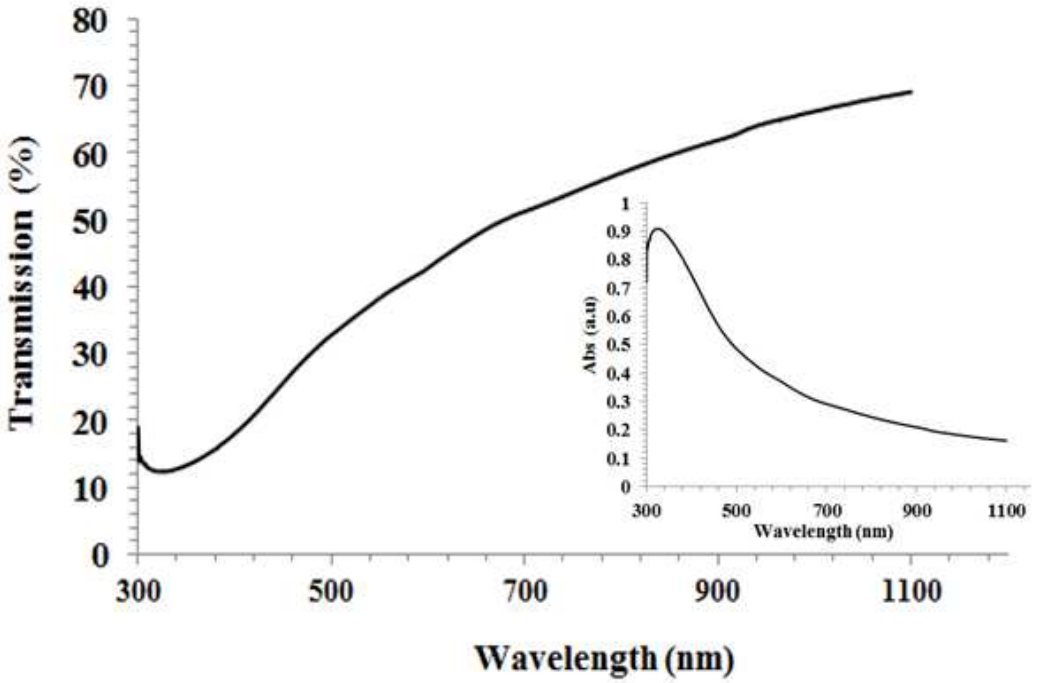
Transmission (%)
80
70
60
50
40
30
20
10
0
300
500
700
900
1100
Wavelength (nm)
Abs (a.u)
1
0.9
0.8
0.7
0.6
0.5
0.4
0.3
0.2
0.1
0
300
500
700
900
1100
Wavelength (nm)

Fig. 6.

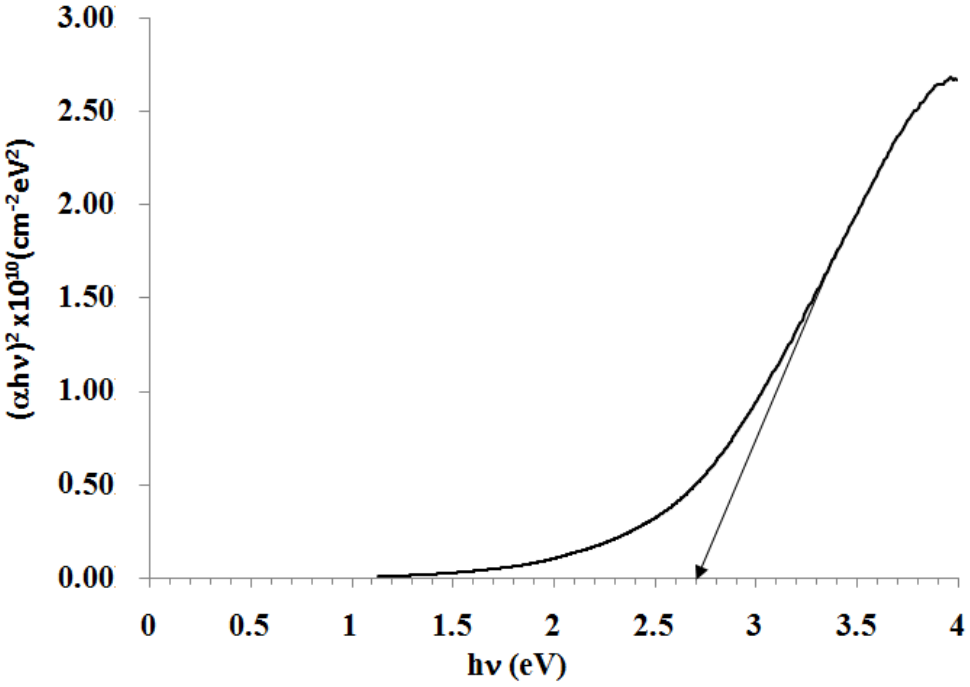
3.00
2.50
2.00
1.50
1.00
0.50
0.00
(αhν)² x10¹⁰(cm⁻²eV²)
0
0.5
1
1.5
2
2.5
3
3.5
4
hν (eV)

Fig. 7.

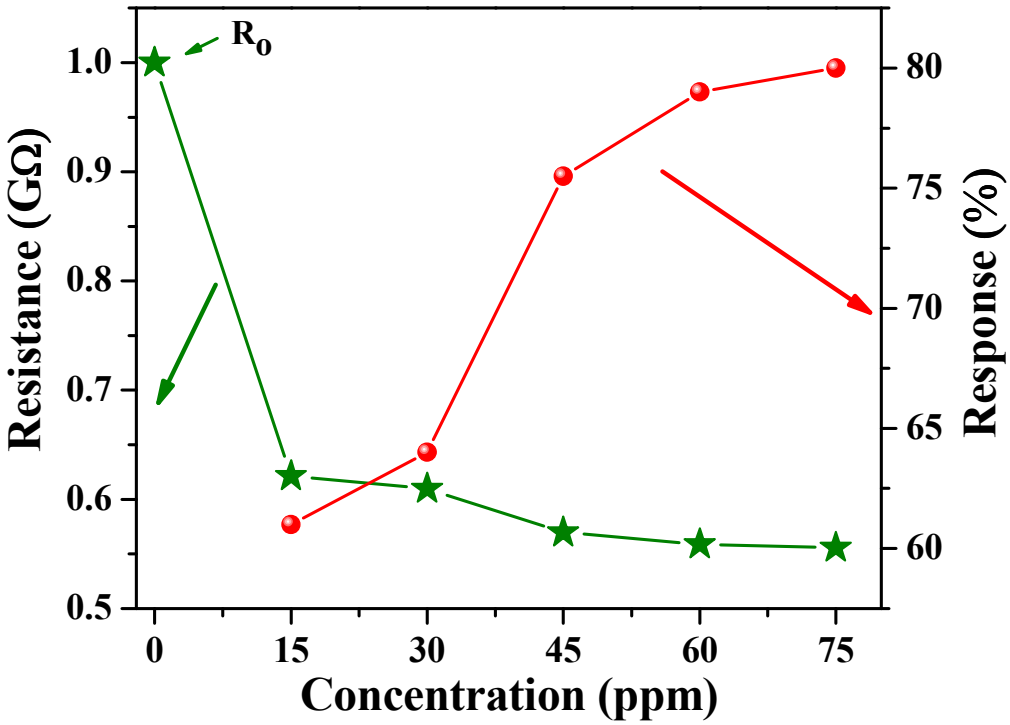
R0
1.0
0.9
0.8
0.7
0.6
0.5
Resistance (GΩ)
80
75
70
65
60
Response (%)
0
15
30
45
60
75
Concentration (ppm)

Fig. 8 (a).

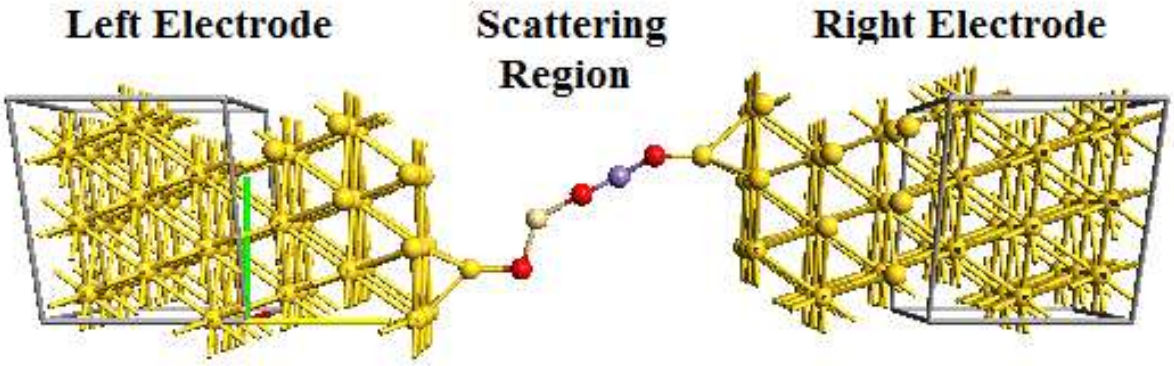

Fig. 8 (b)

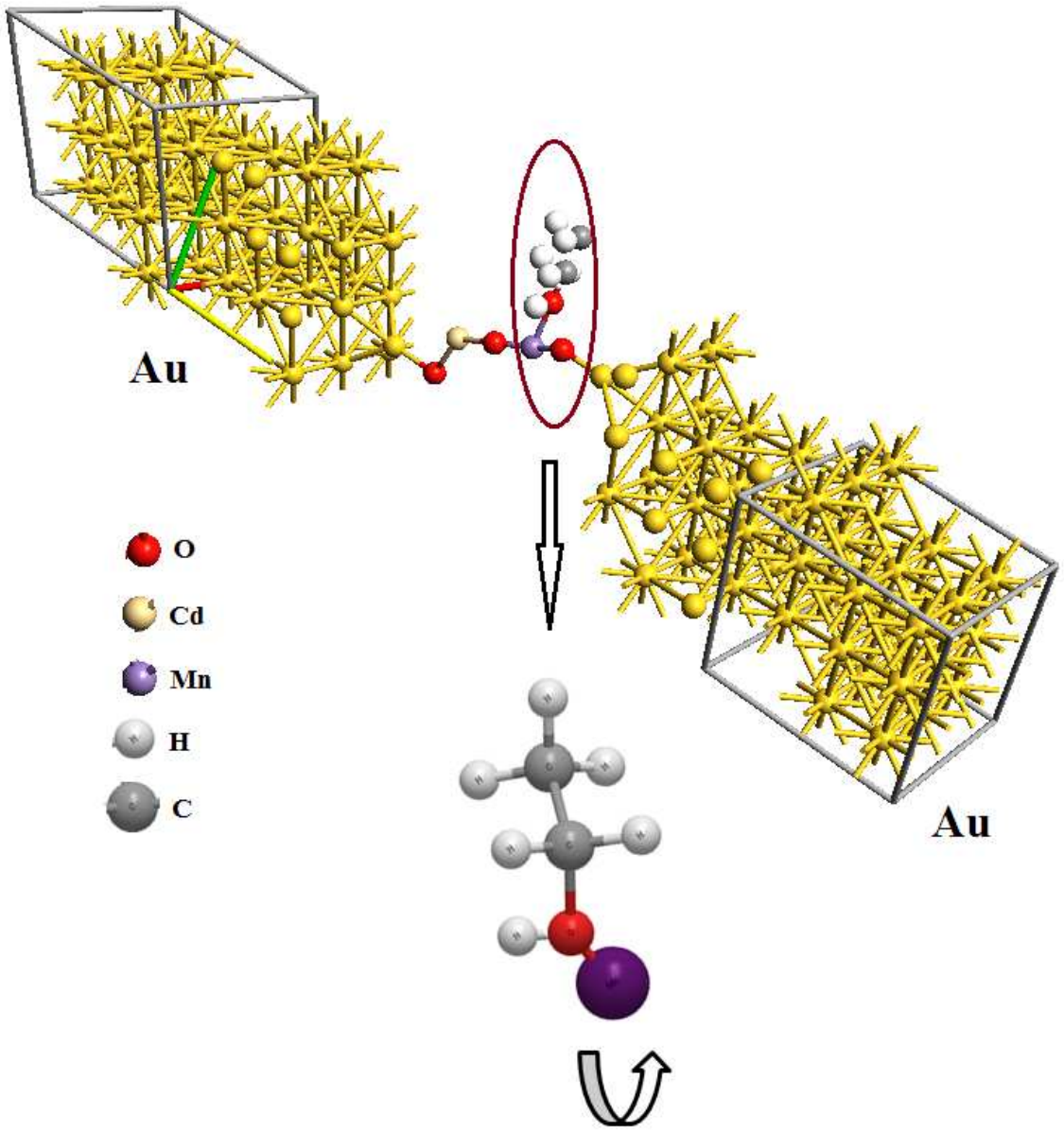

Fig. 9.

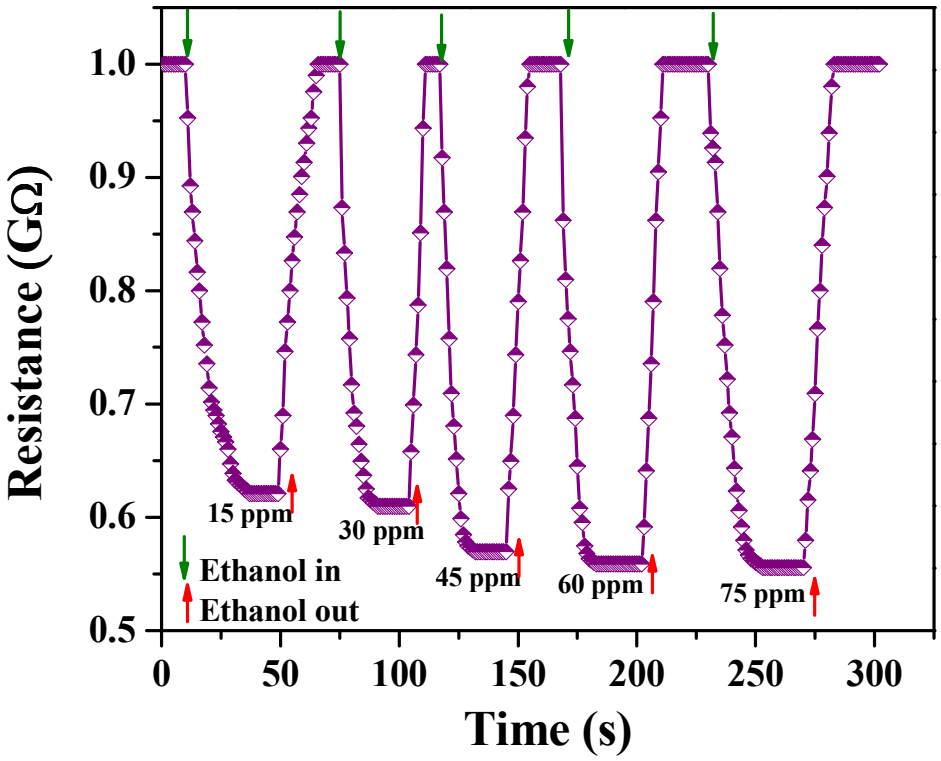
Resistance (GΩ)
1.0
0.9
0.8
0.7
0.6
0.5
0
50
100
150
200
250
300
Time (s)
15 ppm
30 ppm
45 ppm
60 ppm
75 ppm
Ethanol in
Ethanol out

Fig. 10.

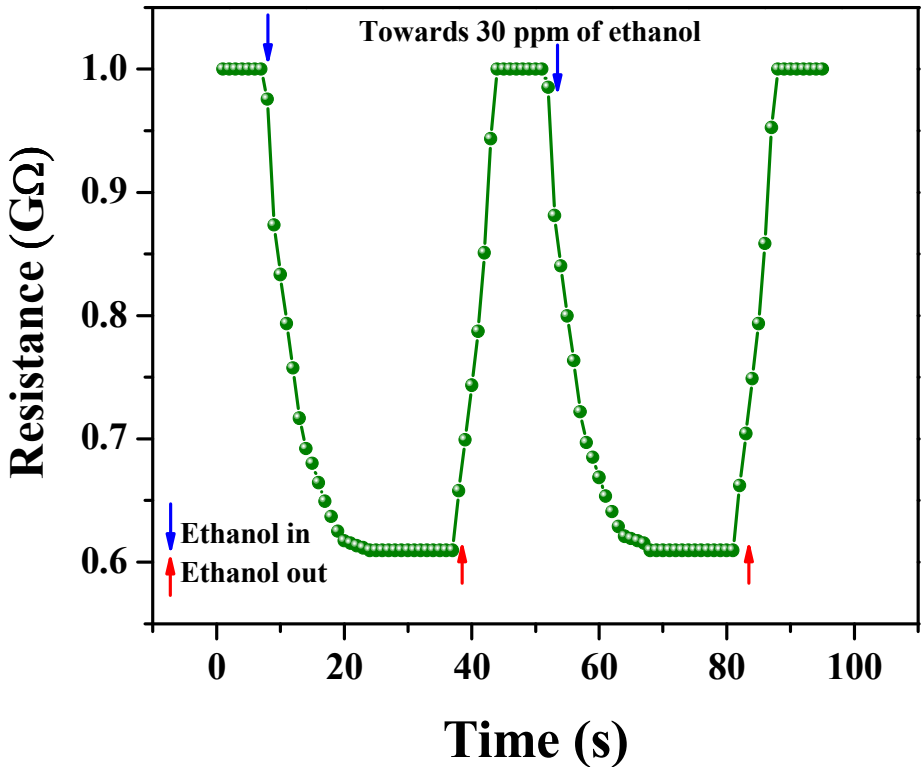
Towards 30 ppm of ethanol
Ethanol in
Ethanol out
Resistance (GΩ)
1.0
0.9
0.8
0.7
0.6
0
20
40
60
80
100
Time (s)

Fig. 11.

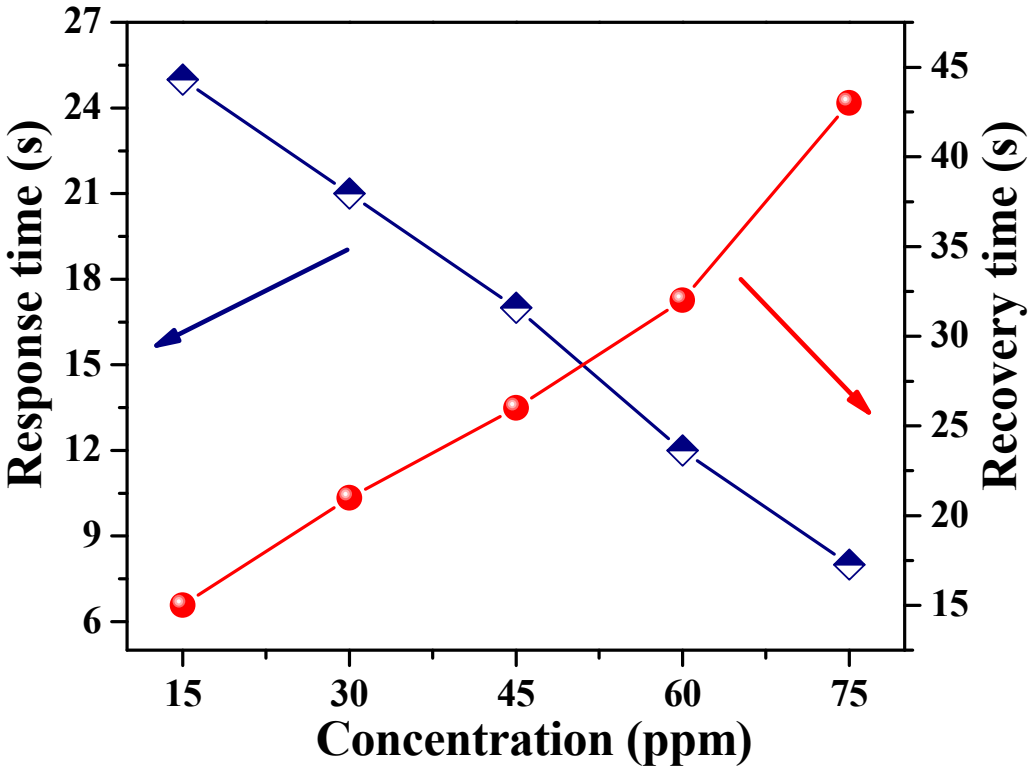
Response time (s)
Recovery time (s)
Concentration (ppm)
27
24
21
18
15
12
9
6
45
40
35
30
25
20
15
15
30
45
60
75

Fig. 12.

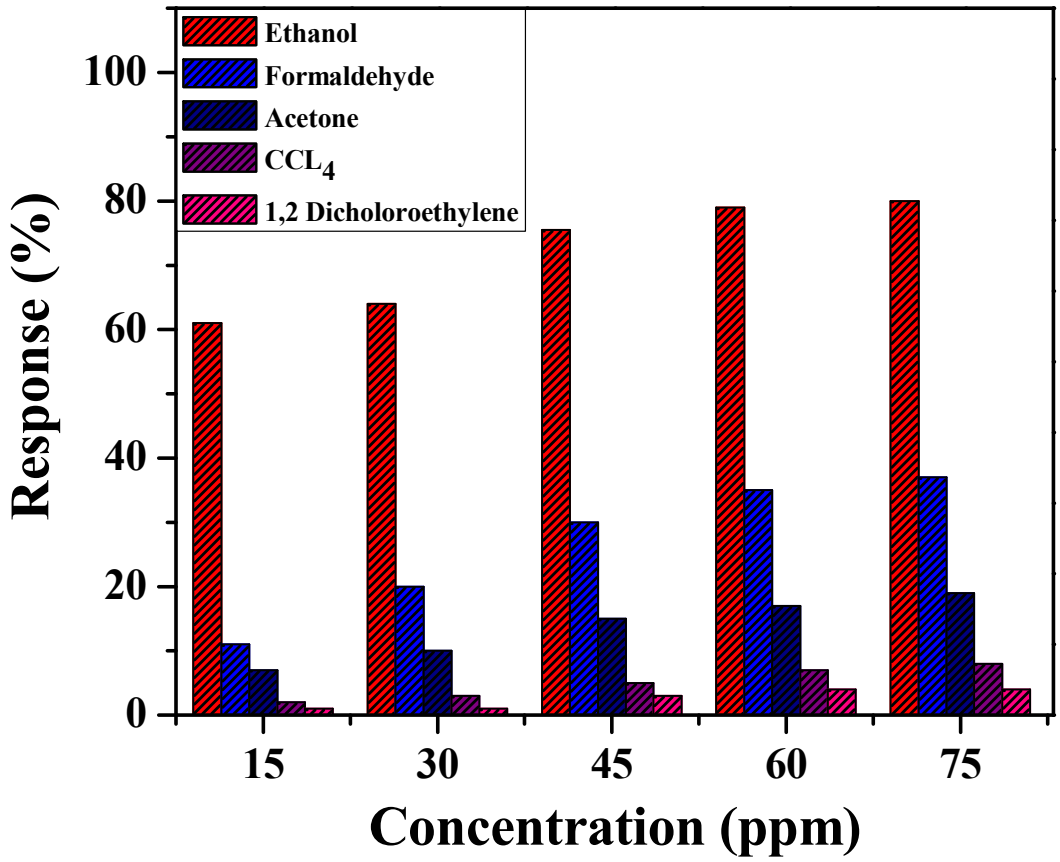
Ethanol
Formaldehyde
Acetone
CCL4
1,2 Dicholoroethylene
Response (%)
0
20
40
60
80
100
15
30
45
60
75
Concentration (ppm)

Fig. 13.

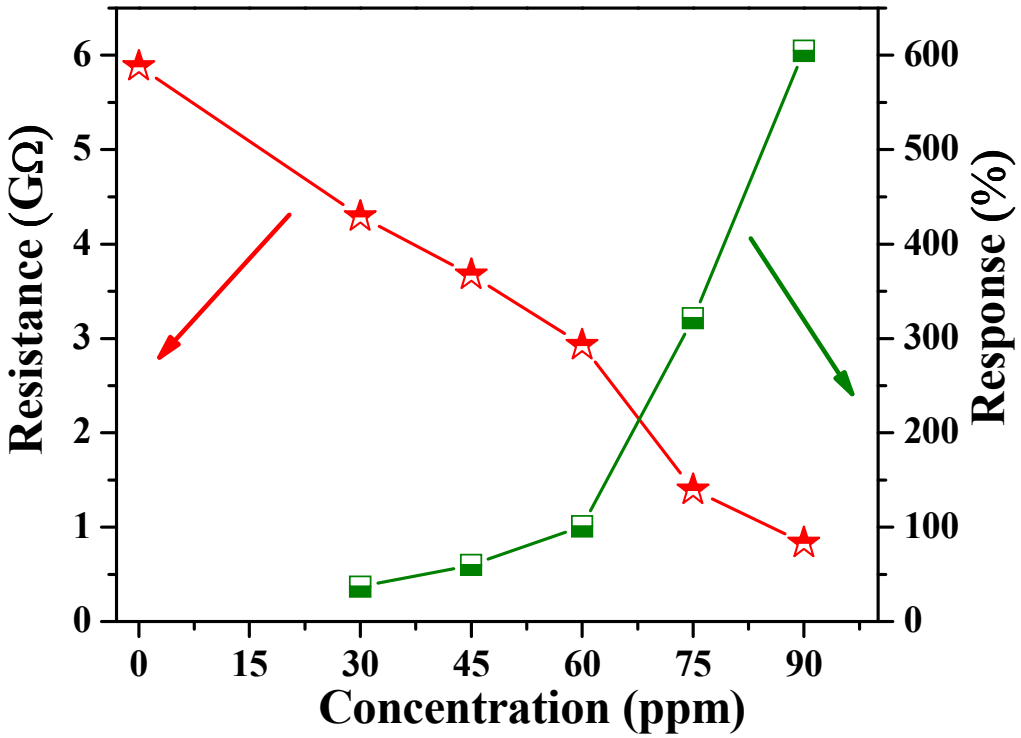
Resistance (GΩ)
Response (%)
Concentration (ppm)
0
1
2
3
4
5
6
0
100
200
300
400
500
600
0
15
30
45
60
75
90

Fig. 14.

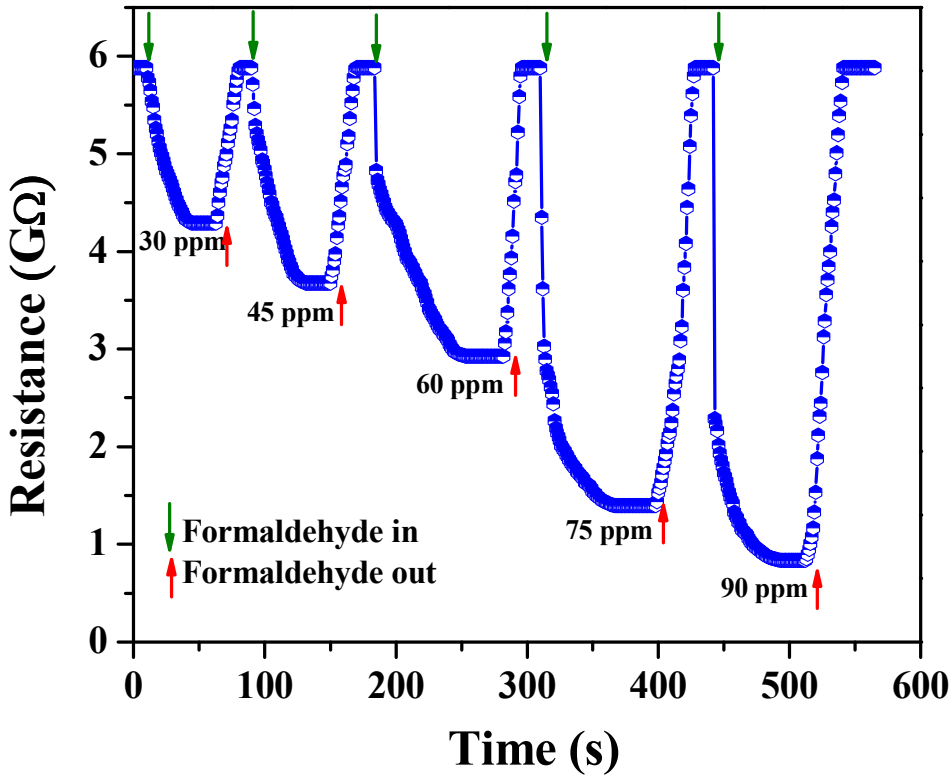
Resistance (GΩ)
Time (s)
0
1
2
3
4
5
6
0
100
200
300
400
500
600
30 ppm
45 ppm
60 ppm
75 ppm
90 ppm
Formaldehyde in
Formaldehyde out

Fig. 15.

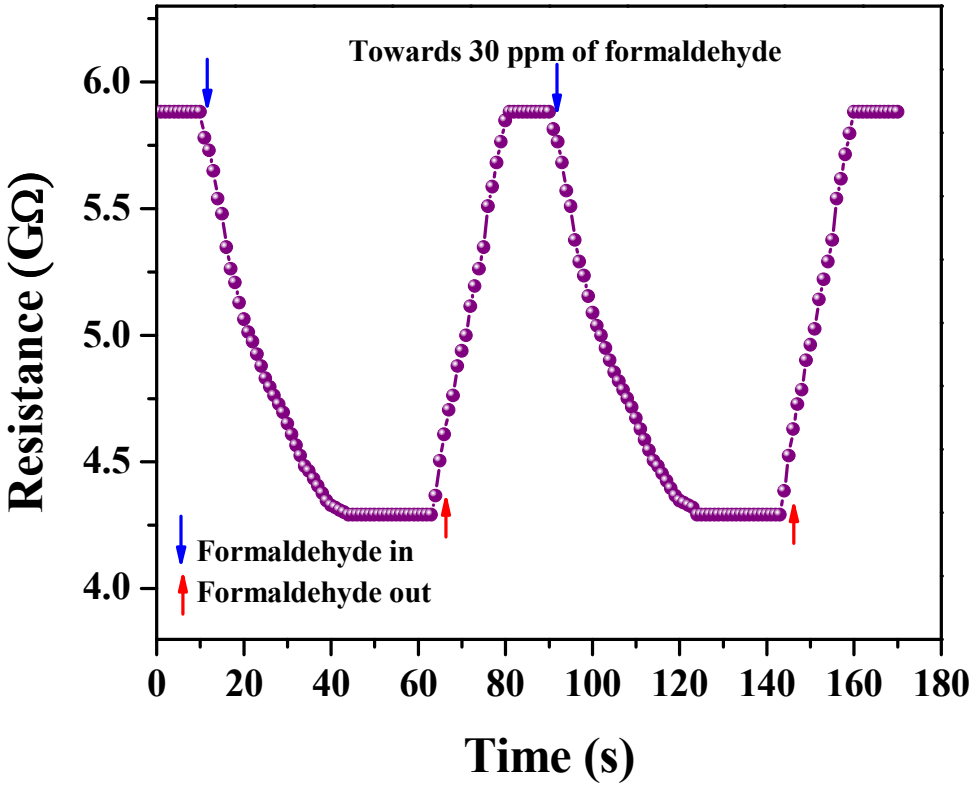
Towards 30 ppm of formaldehyde
Resistance (GΩ)
6.0
5.5
5.0
4.5
4.0
Formaldehyde in
Formaldehyde out
0
20
40
60
80
100
120
140
160
180
Time (s)

Fig. 16.

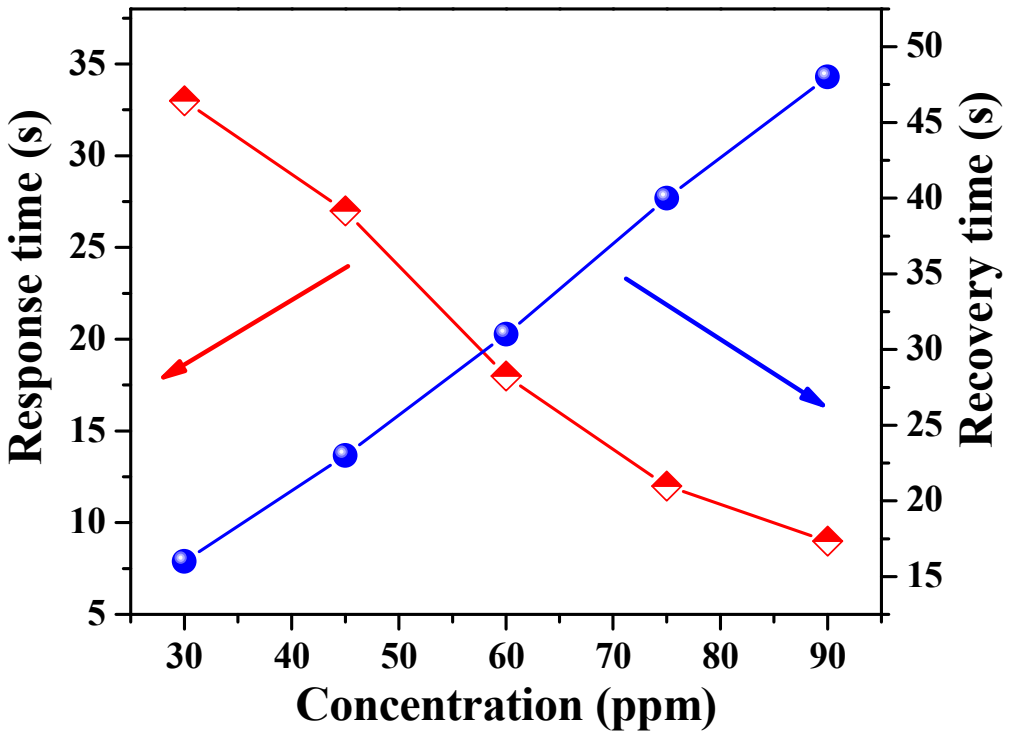
Response time (s)
Recovery time (s)
Concentration (ppm)
35
30
25
20
15
10
5
50
45
40
35
30
25
20
15
30
40
50
60
70
80
90

Fig. 17.

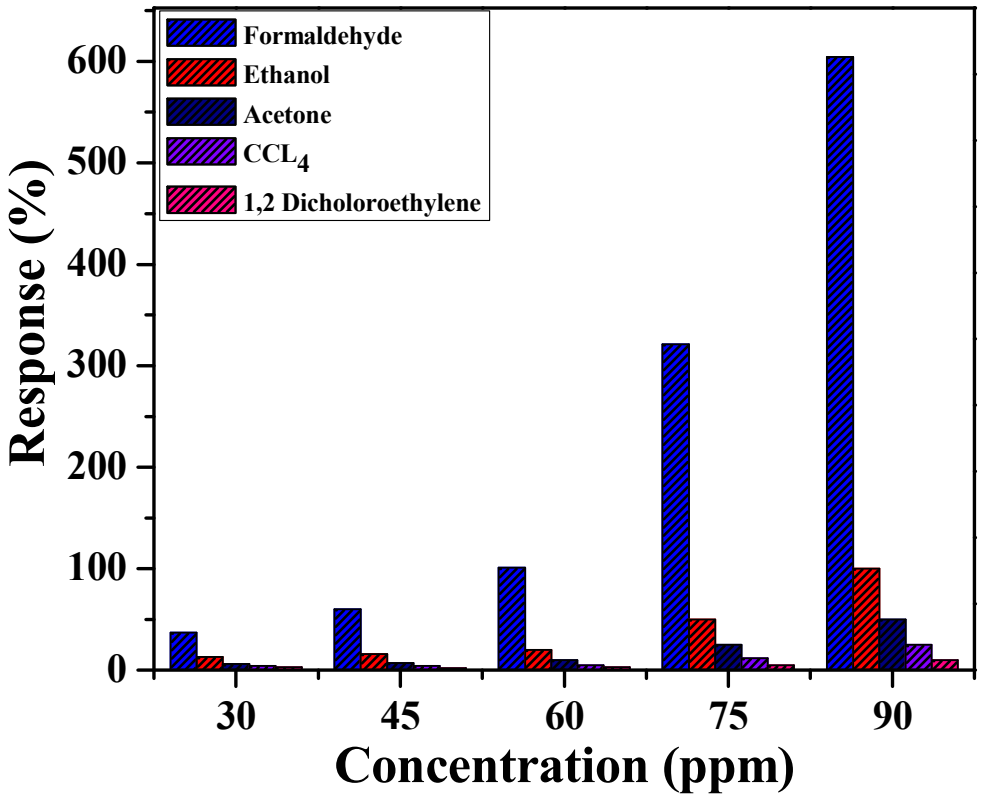
Formaldehyde
Ethanol
Acetone
CCL4
1,2 Dicholoroethylene
Response (%)
0
100
200
300
400
500
600
30
45
60
75
90
Concentration (ppm)

Fig. 18.

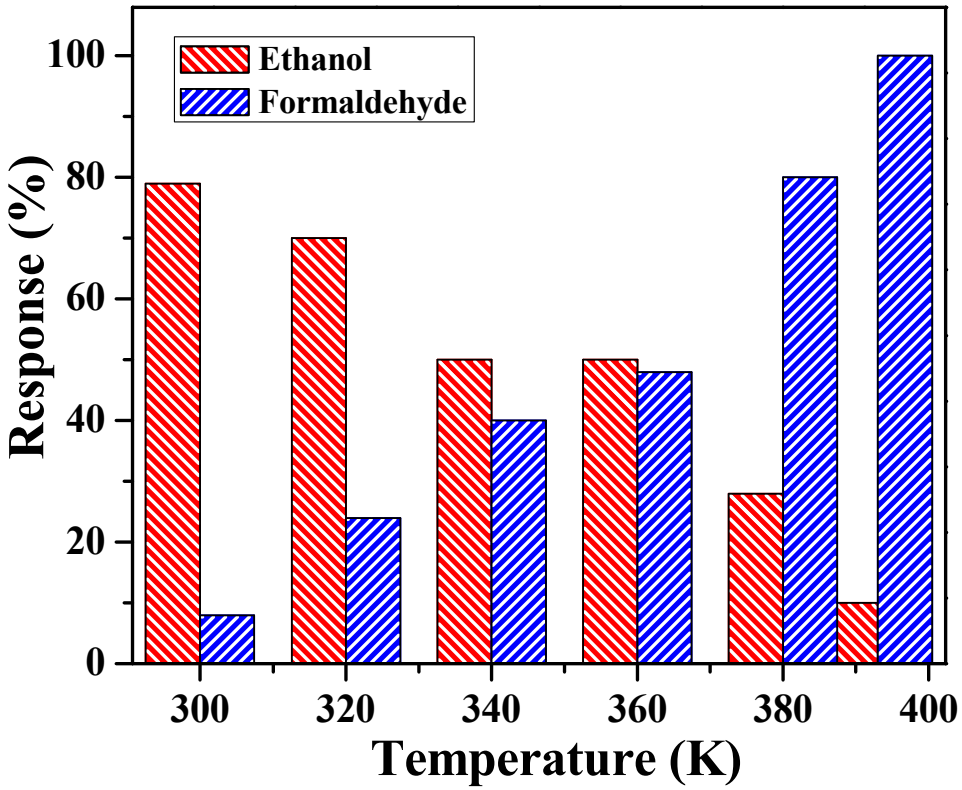
Ethanol
Formaldehyde
Response (%)
0
20
40
60
80
100
300
320
340
360
380
400
Temperature (K)

Fig. 19.

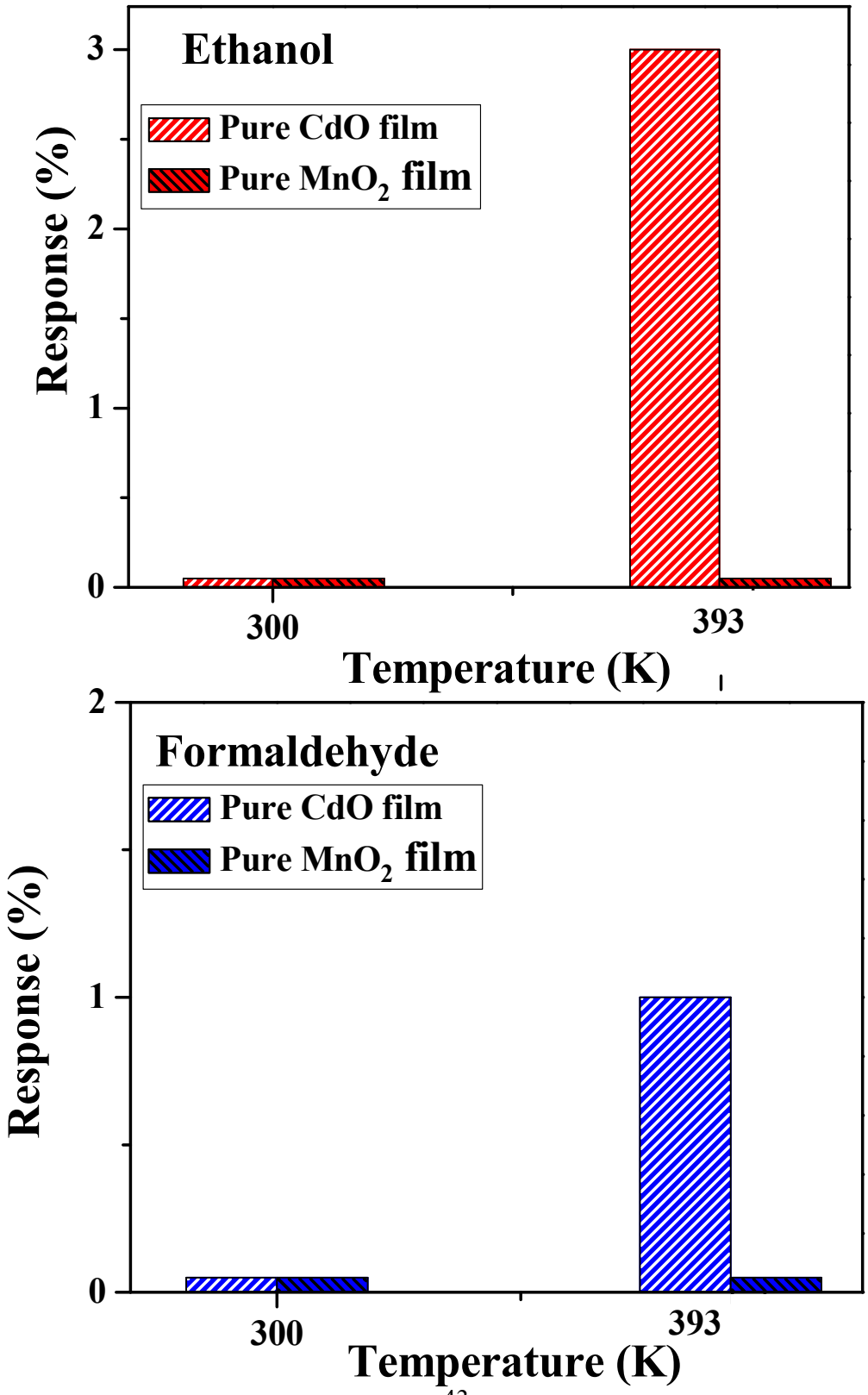
Ethanol
Pure CdO film
Pure MnO2 film
Response (%)
0
1
2
3
300
393
Temperature (K)
Formaldehyde
Pure CdO film
Pure MnO2 film
Response (%)
0
1
2
300
393
Temperature (K)

Fig. 20.

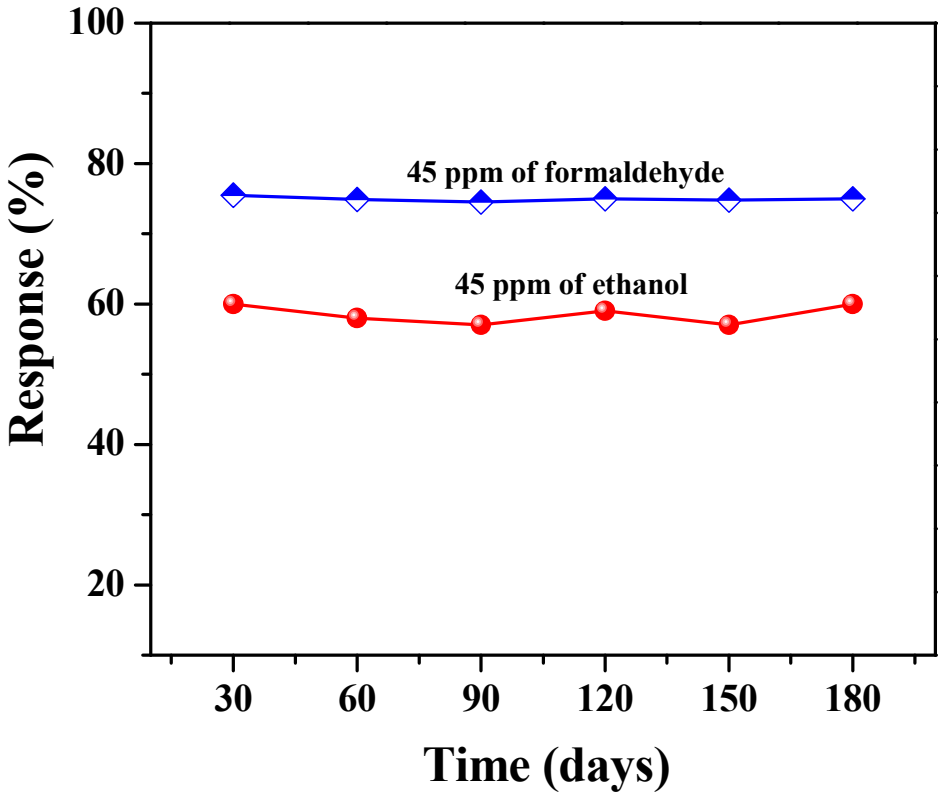
100
80
60
40
20
Response (%)
45 ppm of formaldehyde
45 ppm of ethanol
30
60
90
120
150
180
Time (days)

Fig. 21.

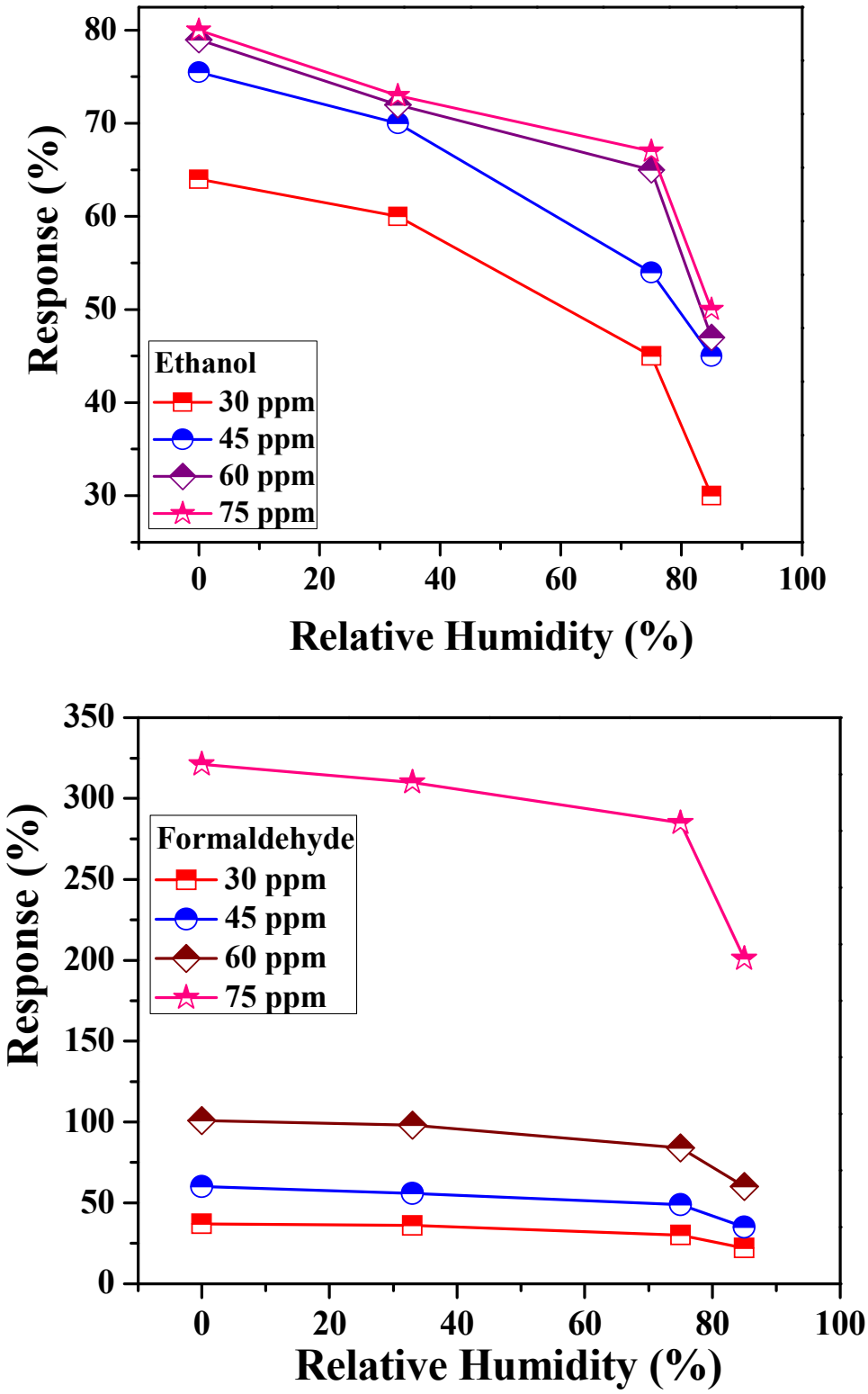
Response (%)
Relative Humidity (%)
Ethanol
30 ppm
45 ppm
60 ppm
75 ppm
Formaldehyde
30 ppm
45 ppm
60 ppm
75 ppm

Table 1.

Metal Oxide	Preparation Method	Detection range (ppm)	Operating temperature (^{o}C)	Response time (s)	Recovery time (s)	Ref.
TiO_2	Anodizing Ti foils	50-1000	250	24-110	6-20	37
TiO_2	Sol-gel dip	10-50	30	65	20	38
In_2O_3	Hydrothermal	50-500	275	16	24	39
ZnO	Electrospinning	10-150	270	7-9	9-11	40
CeO_2	Spray pyrolysis	5-50	100	35	65	41
CuO-In_2O_3	RF sputtering	50-250	300	36-53	149-153	42
ZnO-CdO	Spray pyrolysis	10-150	100	48	60	43
CdO-MnO_2	Spray pyrolysis	15-75	30	15-25	8-42	Present work

Table. 2.

Metal Oxide	**Preparation Method**	**Detection range (ppm)**	**Operating temperature (^{o}C)**	**Response time(s)**	**Recovery time(s)**	**Ref.**
Fe_2O_3-In_2O_3	Electrospinning	1-10000	250	5	25	47
In_2O_3	Ammonolysis and re-oxidation	5-100	420	48	58	48
SnO_2	Screen printing	1-100	210-410	4-57	19-60	49
NiO-SnO_2	Electrospinning	1-10	200	50	80	50
ZnO	Hydrothermal	10-1000	400	41	15	51
CdO-MnO_2	Spray pyrolysis	30-90	120	16-32	8-47	Present work